Theory of nanoscale ripple topographies produced by ion bombardment near the threshold for pattern formation

R. Mark Bradley
Departments of Physics and Mathematics, Colorado State University, Fort Collins, Colorado 80523, USA

(Received 1 June 2020; accepted 13 July 2020; published 31 July 2020)

Nanoscale pattern formation on the surface of a solid that is bombarded with a broad ion beam is studied for angles of ion incidence, θ, just above the threshold angle for ripple formation, θ_c. We carry out a systematic expansion in powers of the small parameter $\epsilon \equiv (\theta - \theta_c)^{1/2}$ and retain all terms up to a given order in ϵ. In the case of two diametrically opposed, obliquely incident beams, the equation of motion close to threshold and at sufficiently long times is rigorously shown to be a particular version of the anisotropic Kuramoto-Sivashinsky equation. We also determine the long-time, near-threshold scaling behavior of the rippled surface's wavelength, amplitude, and transverse correlation length for this case. When the surface is bombarded with a single obliquely incident beam, linear dispersion plays a crucial role close to threshold and dramatically alters the behavior: highly ordered ripples can emerge at sufficiently long times and solitons can propagate over the solid surface. A generalized crater function formalism that rests on a firm mathematical footing is developed and is used in our derivations of the equations of motion for the single and dual beam cases.

DOI: 10.1103/PhysRevE.102.012807

I. INTRODUCTION

Bombarding a solid surface with a broad ion beam can lead to the spontaneous formation of nanoscale patterns on the surface [1]. These patterns include periodic height modulations or "ripples" as well as nanodots arranged in hexagonal arrays of surprising regularity [2–10]. This has sparked widespread interest in using ion sputtering as a means of fabricating nanostructures with feature sizes smaller than those produced by conventional optical lithography.

Much of the theoretical work done in analyzing these patterns has been based on the continuum Bradley-Harper (BH) theory [11], which is in turn based on the Sigmund model of ion sputtering [12]. Bradley and Harper showed that for the Sigmund model, the sputter yield at a point on the surface does not just depend on the local angle of incidence—it also depends on the surface curvature. Because high points on the surface are eroded more slowly than the low points, the curvature dependence of the sputter yield leads to an instability of the solid surface.

The BH theory is linear and, if there is a surface instability, the ripple amplitude grows exponentially with time. In this case, the linear approximation breaks down at some point and nonlinear terms come into play. Cuerno and Barabàsi extended the BH theory to include what they argued are the leading-order nonlinear terms [13]. After transforming to an appropriately chosen moving frame of reference, their equation of motion (EOM) becomes the anisotropic Kuramoto-Sivashinsky (AKS) equation

$$u_t = \Gamma_1 u_{xx} + \Gamma_2 u_{yy} - B\nabla^2\nabla^2 u + \Lambda_1 u_x^2 + \Lambda_2 u_y^2, \quad (1)$$

where $u(x, y, t)$ is the height of the surface above the point (x, y) in the x-y plane at time t; the subscripts x, y, and t denote partial derivatives; the direction of the incident ions has polar angle θ and an azimuthal angle of 180°; and B is the surface diffusivity. The constants Γ_1, Γ_2, Λ_1, and Λ_2 depend on the angle of incidence of the ion beam, θ, and have been computed using the Sigmund theory of sputtering [11,12,14] and atomistic simulations [15,16]. If $\Gamma_1 < \Gamma_2$ and $\Gamma_1 < 0$, ripples with their wave vector parallel to the surface projection of the ion beam direction form; these are called parallel-mode ripples. Conversely, if $\Gamma_2 < \Gamma_1$ and $\Gamma_2 < 0$, perpendicular-mode ripples emerge.

Following the BH approach, Cuerno and Barabàsi assumed that the ripple amplitude is small and the wavelength of the surface ripples, l, is long compared to the characteristic size of a collision cascade a in their derivation of the AKS equation [13]. For a given choice of target material and ion beam, it is unclear *a priori* whether the assumption $l \gg a$ is valid. Moreover, although the assumption that the ripple amplitude is small is valid at early times if the initial surface is nominally flat, it may be invalid at long times.

Since the work of Cuerno and Barabàsi, the theory has been modified in a number of ways because it fails to reproduce a variety of experimentally observed phenomena. A variety of linear and nonlinear terms have been appended to the AKS equation, and in some cases this has led to improved agreement with experiment [14,17–22]. Pearson and Bradley, for example, added the term u_x^3 to the AKS equation [20]. (This term results from a third-order expansion of the sputter yield in powers of the surface slope.) The resulting EOM can lead to the formation of terraced surfaces that are similar to those found in numerous experiments. It has been unclear, however, which terms are negligible and which should be included in the EOM in a given situation.

In the mathematical theory of pattern formation, the nonequilibrium behavior of spatially extended nonlinear systems is studied as a function of a control parameter p

[23,24]. Typically, the system is linearly unstable and a pattern emerges for p greater than a critical value of p which is denoted by p_c, whereas the system is stable and no pattern forms for $p < p_c$. Relatively simple behavior emerges close to the threshold for the pattern formation, i.e., for $p - p_c$ that is small and positive. Near threshold, remarkable analytical progress has been made by carrying out a systematic expansion in the small parameter $p - p_c$. The near-threshold dynamics of the system is universal in the sense that it depends only on the nature of the linear dispersion relation, the dimensionality of the system, and its symmetries. Close to threshold, there is a long characteristic length scale that describes either the pattern itself or slowly varying spatial modulations of it.

For the ion bombardment of a solid, the angle of incidence, θ, is a control parameter that can be directly controlled in an experiment. In addition, there is a critical value of this angle, θ_c. For $\theta > \theta_c$, the surface is unstable and a pattern emerges, while for $\theta < \theta_c$, the surface remains flat. If $\theta - \theta_c$ is positive and is not too large, parallel-mode ripples form. The long length scale near the threshold is the ripple wavelength. The mathematical theory of pattern formation therefore strongly suggests that it would be fruitful to explore the near-threshold behavior of an ion-sputtered surface.

The central goal of this paper is to study the behavior of a solid surface that is bombarded with an ion beam (or ion beams) with an angle of incidence, θ, just above the threshold value θ_c. We carry out a systematic expansion in the small parameter $\epsilon \equiv (\theta - \theta_c)^{1/2}$. The result of this expansion is simplest for the case in which two ion beams are directed onto the solid surface, and these beams have the same ion species, flux, energy, and polar angle of incidence but have azimuthal angles that differ by 180°. We show that for θ just above the critical angle θ_c, the equation of motion has the form

$$u_t = -A_1 u_{xx} + A_2 u_{yy} - B u_{xxxx} + \Lambda_1 u_x^2 \tag{2}$$

to leading order in ϵ. The constant coefficients A_1, A_2, and B are positive but Λ_1 can have either sign. Equation (2) can be viewed as a simplified version of the AKS equation (1). We determine the near-threshold scaling behavior of the ripple wavelength and transverse correlation length. Additionally, we find the scaling behavior of the long-time ripple amplitude and the time needed to approach this steady state.

For the case in which the surface is bombarded by a single obliquely incident ion beam, we are led to the surprising conclusion that the effect of linear dispersion becomes crucial just above the threshold for pattern formation. Since dispersion can lead to the formation of highly ordered parallel-mode ripples [22], this could have important implications for the future prospects of ion sputtering as a nanofabrication tool.

In our derivations of the EOMs for the single and dual beam cases, we develop and utilize a generalized crater function formalism (CFF). The crater function is the average result of many ion impacts at a particular surface point, and so is effectively the Green's function for the problem. The CFF allows us to determine the response of a surface to bombardment with a broad ion beam if the crater function is known [15,25,26]. This approach has the advantage that it takes into account both sputtering and ion-induced mass redistribution [27–29] and does not rely on simple, approximate models of these phenomena like those introduced by Sigmund [12] and Carter and Vishnykov [27]. Our CFF yields explicit expressions for the coefficients A_1, A_2, B, and Λ_1 that appear in Eq. (2). These expressions relate the coefficients to moments of the crater function. Importantly, our CFF is mathematically rigorous and generalizes earlier formulations [15,16,25,26].

This paper is organized as follows. After making some introductory remarks in Sec. II, we introduce the crater function that we employ in Sec. III. In Sec. IV, we develop our generalized crater function formalism. The equation of motion for the case in which diametrically opposed beams are incident on the surface is derived in Sec. V and the scaling behavior close to threshold is found. The case in which a single obliquely incident ion beam is directed into the solid surface is studied in Sec. VI. We discuss our results in Sec. VII and conclude in Sec. VIII. We demonstrate that the expressions that our generalized CFF yields for the coefficients A_1, A_2, and Λ_1 agree with previous results [20,26] in the Appendix.

II. PRELIMINARY CONSIDERATIONS

We begin by considering the bombardment of a solid elemental material with a single broad beam of noble gas ions before moving on to the case in which two diametrically opposed beams are incident on the surface. The material may be amorphous or crystalline. If the material is initially crystalline, we assume that a layer at the surface of the solid is amorphized by the ion bombardment. Additionally, we take the sample temperature to be low enough that the effect of thermally activated surface diffusion is negligible compared to the effect of ion-induced surface viscous flow [30].

If the beam energy is not too high, implanted noble gas ions will be present only within a shallow surface layer. The ions diffuse within the solid and usually desorb or are sputtered away once they reach its surface. For simplicity, we make the customary assumption that the concentration of implanted noble gas ions is negligibly small [31].

The sample surface is taken to be nominally flat before the irradiation begins. We define the $\hat{\boldsymbol{z}}$ direction to be the global vertical, normal to the macroscopic surface. The unit vector $\hat{\boldsymbol{x}}$ is taken to be the direction of the projection of the incident ion beam onto the macroscopic surface, and $\hat{\boldsymbol{y}}$ is taken to be normal to the x-z plane. The incident ion flux is $\boldsymbol{J} = -J\hat{\boldsymbol{e}}$, where $\hat{\boldsymbol{e}} \equiv -\hat{\boldsymbol{x}} \sin\theta + \hat{\boldsymbol{z}} \cos\theta$ and the angle of incidence, θ, is the angle between the global vertical and the incident beam.

We employ a continuum description of the surface dynamics in which the position of an arbitrary point on the surface is given by $\boldsymbol{r} = x\hat{\boldsymbol{x}} + y\hat{\boldsymbol{y}} + h(x, y, t)\hat{\boldsymbol{z}}$, where $h(x, y, t)$ is the height of the point above the x-y plane at time t. The surface height h is obtained by coarse-graining the detailed microscopic surface configuration and is assumed to be a smoothly varying function of its arguments x, y, and t.

III. THE CRATER FUNCTION

The crater function describes the average effect of a single ion impact on the morphology of the solid surface. In this section, we place the origin O at the point of impact and, for

the sake of simplicity, we do not display the time t in the list of arguments of h.

There are many possible configurations of atoms beneath the solid surface that are consistent with a given coarse-grained surface height $h = h(x, y)$. The form of the crater that is produced by the ion impact depends on the detailed microscopic arrangement of atoms beneath the surface of the solid. The crater we employ is a statistical average of craters that result from ion impacts on the many different possible microscopic arrangements of atoms beneath the given coarse-grained surface.

The value of the crater function f at the point (x, y) is defined to be minus the average change in the surface height h above the point (x, y) in the x-y plane as a result of a single ion impact at $x = y = 0$. The crater function f depends on x, y, and the angle of incidence, θ. It also depends on the shape of the entire surface, or, equivalently, on all of the spatial derivatives of $h(x, y)$ evaluated at $x = y = 0$. We write

$$f = f(x, y, \theta; h_x, h_y, h_{xx}, h_{xy}, h_{yy}, h_{xxx}, h_{xxy}, h_{xyy}, h_{yyy}, h_{xxxx}, \ldots). \tag{3}$$

The partial derivatives of h that appear on the right-hand side of Eq. (3) are all to be evaluated at $x = y = 0$. We assume that f is known *a priori* from another theory or from atomistic simulations.

In addition to the coordinates x, y, and z, we utilize a second set of coordinates with its origin at the point O. We define the vector $\hat{\boldsymbol{n}}$ to be the local surface normal at O and $\hat{\boldsymbol{t}}_\xi$ to be the local downbeam direction projected onto the surface. Explicitly,

$$\hat{\boldsymbol{n}} = \frac{\hat{\boldsymbol{z}} - \boldsymbol{\nabla} h}{\sqrt{1 + (\boldsymbol{\nabla} h)^2}} \tag{4}$$

and

$$\hat{\boldsymbol{t}}_\xi = \frac{-\boldsymbol{J} + (\boldsymbol{J} \cdot \hat{\boldsymbol{n}})\hat{\boldsymbol{n}}}{|-\boldsymbol{J} + (\boldsymbol{J} \cdot \hat{\boldsymbol{n}})\hat{\boldsymbol{n}}|}. \tag{5}$$

$\hat{\boldsymbol{t}}_\eta$ is defined to be the cross product of $\hat{\boldsymbol{n}}$ and $\hat{\boldsymbol{t}}_\xi$. The unit vectors $\hat{\boldsymbol{t}}_\xi$, $\hat{\boldsymbol{t}}_\eta$, and $\hat{\boldsymbol{n}}$ form an orthonormal basis and $\hat{\boldsymbol{t}}_\xi$ and $\hat{\boldsymbol{t}}_\eta$ are tangent to the surface at O. We define ξ, η, and ζ to be the coordinates along the directions $\hat{\boldsymbol{t}}_\xi$, $\hat{\boldsymbol{t}}_\eta$, and $\hat{\boldsymbol{n}}$, respectively, and let $H(\xi, \eta)$ denote the height of the solid surface above the point (ξ, η) in the ξ-η plane. The local angle of ion incidence, which will be denoted by ϕ, is given by $\cos\phi = \hat{\boldsymbol{e}} \cdot \hat{\boldsymbol{n}}$.

In previous formulations of the CFF [16,25,26], the crater function F that is employed is defined relative to the coordinate system with coordinates ξ, η, and ζ. The value of F at the point (ξ, η) is defined to be minus the average change in the local surface height H above the point (ξ, η) in the ξ-η plane as a result of a single ion impact at $\xi = \eta = 0$. F depends on ξ, η, and the local angle of incidence, ϕ. It also depends on all of the spatial derivatives of H evaluated at $\xi = \eta = 0$. Since H_ξ and H_η vanish for $\xi = \eta = 0$, we write

$$F = F(\xi, \eta, \phi; H_{\xi\xi}, H_{\xi\eta}, H_{\eta\eta}, H_{\xi\xi\xi}, \ldots). \tag{6}$$

The partial derivatives of H that appear on the right-hand side of Eq. (3) are evaluated at $\xi = \eta = 0$.

As we shall see, it is much simpler to develop the CFF that is based on the crater function f than it was to develop the CFF based on the crater function F. This new approach enables us to determine the leading-order effect of nonlinearities and higher-order spatial derivatives on the surface evolution. The approach introduced in this paper is simpler because it removes the need to transform from the local coordinate system (ξ, η, ζ) at the point of ion impact to the global or laboratory coordinate system (x, y, z).

There is an important special case we should touch on. If $h_x = h_y = 0$, then the coordinate systems (x, y, z) and (ξ, η, ζ) coincide: $H = h$ and $\phi = \theta$. It follows that

$$F(x, y, \theta; h_{xx}, h_{xy}, h_{yy}, h_{xxx}, \ldots) = f(x, y, \theta; 0, 0, h_{xx}, h_{xy}, h_{yy}, h_{xxx}, \ldots) \tag{7}$$

and so the crater function F that was previously employed is a special case of our crater function f.

We take the crater function f to be evaluated at a time long enough after the ion impact that essentially all ion-induced motion has ceased. It therefore takes into account sputtering, mass redistribution, and ion-induced surface viscous flow. When a broad beam is incident on the surface, we assume that the ion flux is low enough that all ion-induced motion near a point of impact, **P**, has ended before another ion strikes the surface in the vicinity of **P**.

IV. THE GENERALIZED CRATER FUNCTION FORMALISM

We begin this section by finding h_t at an arbitrary point $\mathbf{P}_0$ on the solid surface for all times $t \geqslant 0$. The case in which a single broad beam of noble gas ions is incident on the solid is considered. We now find it convenient to place the origin O at the position of $\mathbf{P}_0$ at time t. The origin is taken to be stationary, and it so will remain fixed as the surface point $\mathbf{P}_0$ moves either up or down.

The flux of ions through a surface element dA centered on $\boldsymbol{r}$ is $J\hat{\boldsymbol{e}} \cdot \hat{\boldsymbol{n}} dA$, where the surface normal $\hat{\boldsymbol{n}}$ is given by Eq. (4) and $dA = \sqrt{1 + (\nabla h)^2}\, dx\, dy$. Each arriving ion produces a crater which changes the height of the surface point $\mathbf{P}_0$. It follows that the value of h_t at $x = y = 0$ is given by

$$h_t = -J \int dx \int dy f(-x, -y, \theta; h_x, h_y, h_{xx}, h_{xy}, h_{yy}, \ldots) \times (\cos\theta + h_x \sin\theta). \tag{8}$$

All of the spatial derivatives of h that appear in the integrand on the right-hand side of Eq. (8) are evaluated at the point (x, y) in the x-y plane.

Although Eq. (8) gives h_t and completely specifies the dynamics of the surface, it is an exceedingly complicated integrodifferential equation. It becomes much simpler when $\epsilon \equiv (\theta - \theta_c)^{1/2}$ is small and positive, however. Let v_0 be the rate the surface recedes if it is perfectly planar, and set $h(x, y, t) = -v_0 t + u(x, y, t)$. We seek solutions to Eq. (8) of the form

$$u(x, y, t) = \epsilon^2 U(X, Y, T), \tag{9}$$

where

$$X \equiv \epsilon x, \quad Y \equiv \epsilon^2 y, \quad \text{and} \quad T \equiv \epsilon^4 t. \tag{10}$$

X, Y, and T are the "slow" variables and x, y, and t are the corresponding "fast" variables. Heuristically speaking, Eq. (9) says that close to the critical angle θ_c, the amplitude of the surface disturbance is small and it varies slowly in space and time. In addition, the spatial variation in the y direction is more gradual than in the x direction. An *a posteriori* justification for adopting the scaling given by Eqs. (9) and (10) will be obtained once we have arrived at an EOM that is well behaved in the $\epsilon \to 0$ limit for the case in which diametrically opposed beams are incident on the target's surface.

The crater function f depends on the fast spatial variables x and y since it varies over distances on the order of the characteristic size of a collision cascade a. It is also a function of the slow spatial variables X and Y because it depends on the spatial derivatives of h. These derivatives vary only over distances comparable to the ripple wavelength l, and l is much larger than a close to threshold.

We now insert Eq. (9) into Eq. (8) and expand in powers of ϵ. Throughout the calculation, we retain terms up to sixth order in ϵ. We define

$$f_0(x,y,\theta) \equiv f(x,y,\theta;0,0,\ldots), \tag{11}$$

$$f_1(x,y,\theta) \equiv \frac{\partial}{\partial h_x} f(x,y,\theta;h_x,0,0,\ldots)\Big|_{h_x=0}, \tag{12}$$

$$f_2(x,y,\theta) \equiv \frac{\partial}{\partial h_y} f(x,y,\theta;0,h_y,0,0,\ldots)\Big|_{h_y=0}, \tag{13}$$

$$f_3(x,y,\theta) \equiv \frac{\partial}{\partial h_{xx}} f(x,y,\theta;0,0,h_{xx},0,0,\ldots)\Big|_{h_{xx}=0}, \tag{14}$$

and so on. Similarly, for positive integers i and j, $f_{i,j}(x,y,\theta)$ denotes the partial derivative of $f(x,y,\theta;h_x,h_y,h_{xx},h_{xy},\ldots)$ with respect to the ith and jth arguments that appear after the semicolon, evaluated for all the arguments after the semicolon set equal to zero. For example,

$$f_{1,3}(x,y,\theta) \equiv \frac{\partial}{\partial h_x}\frac{\partial}{\partial h_{xx}} f(x,y,\theta;h_x,0,h_{xx},0,0,\ldots)\Big|_{h_x=h_{xx}=0}. \tag{15}$$

Equation (8) becomes

$$\begin{aligned}
&-J^{-1}(-v_0+\epsilon^6 U_T)\\
&\quad=\cos\theta\int dx\int dy\Big[f_0(-x,-y,\theta)+\epsilon^3 U_X f_1(-x,-y,\theta)\\
&\qquad+\epsilon^4 U_Y f_2(-x,-y,\theta)+\epsilon^4 U_{XX} f_3(-x,-y,\theta)\\
&\qquad+\epsilon^5 U_{XY} f_4(-x,-y,\theta)+\epsilon^6 U_{YY} f_5(-x,-y,\theta)\\
&\qquad+\epsilon^5 U_{XXX} f_6(-x,-y,\theta)+\epsilon^6 U_{XXY} f_7(-x,-y,\theta)\\
&\qquad+\epsilon^6 U_{XXXX} f_{10}(-x,-y,\theta)+\frac{1}{2}\epsilon^6 U_X^2 f_{1,1}(-x,-y,\theta)\Big]\\
&\qquad+\sin\theta\int dx\int dy\big[\epsilon^3 U_X f_0(-x,-y,\theta)\\
&\qquad+\epsilon^6 U_X^2 f_1(-x,-y,\theta)\big].
\end{aligned} \tag{16}$$

On the left-hand side of Eq. (16), $U_T = U_T(0,0,T)$. All of the spatial derivatives of U that appear on the right-hand side of Eq. (16) have the arguments X, Y, and T.

We next carry out a Taylor-series expansion of $U(X,Y,T)$ about the point $X = Y = 0$: we set

$$U(X,Y,T) = \sum_{n=0}^{\infty}\sum_{m=0}^{\infty} S_{n,m}(T)\frac{X^n Y^m}{n!\,m!}, \tag{17}$$

where

$$S_{n,m}(T) \equiv \frac{\partial^{n+m}U}{\partial X^n \partial Y^m}(0,0,T). \tag{18}$$

We also introduce new dummy variables of integration, $\tilde{x} = -x$ and $\tilde{y} = -y$, in Eq. (16) and then drop the tildes. So that the resulting EOM may be written succinctly, we define the crater function moments

$$M^{n,m} \equiv \iint x^n y^m f_0(x,y,\theta)\,dx\,dy. \tag{19}$$

We also let

$$M_i^{n,m} \equiv \iint x^n y^m f_i(x,y,\theta)\,dx\,dy \tag{20}$$

and

$$M_{i,j}^{n,m} \equiv \iint x^n y^m f_{i,j}(x,y,\theta)\,dx\,dy \tag{21}$$

for nonnegative integers n and m and positive integers i and j. After a considerable amount of algebra, we find that

$$v_0 = JM^{0,0}\cos\theta \tag{22}$$

and

$$\begin{aligned}
J^{-1}\epsilon^6 U_T &= \epsilon^3 C_1 S_{1,0}+\epsilon^4 C_2 S_{0,1}+\epsilon^4 C_{11} S_{2,0}+\epsilon^5 C_{12} S_{1,1}\\
&\quad+\epsilon^6 C_{22} S_{0,2}+\epsilon^5 C_{111} S_{3,0}+\epsilon^6 C_{112} S_{2,1}\\
&\quad+\epsilon^6 C_{1111} S_{4,0}+\epsilon^6 \lambda_1 S_{1,0}^2.
\end{aligned} \tag{23}$$

Here

$$C_1 = -\big(M_1^{0,0}\cos\theta + M^{0,0}\sin\theta\big), \tag{24}$$

$$C_2 = -M_2^{0,0}\cos\theta, \tag{25}$$

$$C_{11} = \big(M_1^{1,0} - M_3^{0,0}\big)\cos\theta + M^{1,0}\sin\theta, \tag{26}$$

$$C_{12} = \big(M_1^{0,1} + M_2^{1,0} - M_4^{0,0}\big)\cos\theta + M^{0,1}\sin\theta, \tag{27}$$

$$C_{22} = \big(M_2^{0,1} - M_5^{0,0}\big)\cos\theta, \tag{28}$$

$$C_{111} = \big(-\tfrac{1}{2}M_1^{2,0} + M_3^{1,0} - M_6^{0,0}\big)\cos\theta - \tfrac{1}{2}M^{2,0}\sin\theta, \tag{29}$$

$$\begin{aligned}
C_{112} &= \big(-M_1^{1,1} - \tfrac{1}{2}M_2^{2,0} + M_3^{0,1} + M_4^{1,0} - M_7^{0,0}\big)\cos\theta\\
&\quad - M^{1,1}\sin\theta,
\end{aligned} \tag{30}$$

$$\begin{aligned}
C_{1111} &= \big(\tfrac{1}{6}M_1^{3,0} - \tfrac{1}{2}M_3^{2,0} + M_6^{1,0} - M_{10}^{0,0}\big)\cos\theta\\
&\quad + \tfrac{1}{6}M^{3,0}\sin\theta,
\end{aligned} \tag{31}$$

and

$$\lambda_1 = -\big(\tfrac{1}{2}M_{1,1}^{0,0}\cos\theta + M_1^{0,0}\sin\theta\big). \tag{32}$$

Recalling the definition of $S_{n,m}$ [Eq. (18)], Eq. (23) becomes

$$J^{-1}\epsilon^6 U_T = \epsilon^3 C_1 U_X + \epsilon^4 C_2 U_Y + \epsilon^4 C_{11} U_{XX} + \epsilon^5 C_{12} U_{XY} + \epsilon^6 C_{22} U_{YY} + \epsilon^5 C_{111} U_{XXX} + \epsilon^6 C_{112} U_{XXY} + \epsilon^6 C_{1111} U_{XXXX} + \epsilon^6 \lambda_1 U_X^2, \quad (33)$$

where all of the partial derivatives of U are evaluated at $X = Y = 0$. Equation (33) holds for $X = Y = 0$. However, because we placed the origin at an arbitrary surface point, this equation is actually valid for all X and Y.

The equation of motion must be invariant under the transformation $Y \to -Y$. As a result, the coefficients C_2, C_{12}, and C_{112} must be zero. This is true because $M_2^{0,0}$, $M_1^{0,1}$, $M_2^{1,0}$, $M_4^{0,0}$, $M^{0,1}$, $M_1^{1,1}$, $M_2^{2,0}$, $M_3^{0,1}$, $M_4^{1,0}$, $M_7^{0,0}$, and $M^{1,1}$ all vanish. It is straightforward to verify that these statements are true. For example, $M^{0,1}$, $M^{1,1}$, $M_1^{0,1}$, $M_1^{1,1}$, and $M_3^{0,1}$ are all zero because their integrands are odd functions of y. Equation (33) reduces to

$$J^{-1}U_T = \epsilon^{-3} C_1 U_X + \epsilon^{-2} C_{11} U_{XX} + \epsilon^{-1} C_{111} U_{XXX} + C_{22} U_{YY} + C_{1111} U_{XXXX} + \lambda_1 U_X^2. \quad (34)$$

Note that all of the coefficients on the right-hand side of Eq. (34) depend on the angle of incidence, θ.

The EOM (34) becomes

$$J^{-1}u_t = C_1 u_x + C_{11} u_{xx} + C_{22} u_{yy} + C_{111} u_{xxx} + C_{1111} u_{xxxx} + \lambda_1 u_x^2 \quad (35)$$

when written in terms of the original, unscaled variables. The coefficients on the right-hand side of Eq. (35) are related to the crater function moments by Eqs. (24), (26), (28), (29), (31), and (32). Our expressions for C_1, C_{11}, C_{22}, and λ_1 agree with the results derived in Refs. [20,26], as shown in the Appendix.

V. EQUATION OF MOTION FOR DIAMETRICALLY OPPOSED BEAMS

We now turn our attention to the problem in which there are two diametrically opposed beams, each with ion flux $J/2$. (Recall that the beams have the same polar angle but their azimuthal angles differ by 180°.) If only the beam that is incident from the left is present, the EOM is Eq. (34) with J replaced by $J/2$:

$$U_T = \frac{J}{2}\left(\epsilon^{-3} C_1 U_X + \epsilon^{-2} C_{11} U_{XX} + \epsilon^{-1} C_{111} U_{XXX} + C_{22} U_{YY} + C_{1111} U_{XXXX} + \lambda_1 U_X^2\right). \quad (36)$$

Conversely, if only the beam that is incident from the right is present, the EOM is Eq. (36) with X replaced by $-X$:

$$U_T = \frac{J}{2}\left(-\epsilon^{-3} C_1 U_X + \epsilon^{-2} C_{11} U_{XX} - \epsilon^{-1} C_{111} U_{XXX} + C_{22} U_{YY} + C_{1111} U_{XXXX} + \lambda_1 U_X^2\right). \quad (37)$$

To get U_T when both beams are turned on, we take the sum of the right-hand sides of Eqs. (36) and (37) to yield

$$U_T = J\left(\epsilon^{-2} C_{11} U_{XX} + C_{22} U_{YY} + C_{1111} U_{XXXX} + \lambda_1 U_X^2\right). \quad (38)$$

This is the equation of motion for the surface for the case in which diametrically opposed beams with equal ion fluxes are simultaneously incident on the target. Note that in addition to being invariant under the transformation $Y \to -Y$, Eq. (38) is invariant under $X \to -X$, as it must be.

Equation (38) holds for θ just above the critical angle θ_c, i.e., for small $\epsilon = (\theta - \theta_c)^{1/2}$. C_{11} is positive for $\theta < \theta_c$, zero for $\theta = \theta_c$, and negative for $\theta > \theta_c$, at least provided that θ is not too large. For θ close to the critical angle, $C_{11} \cong -A_{11}(\theta - \theta_c) = -A_{11}\epsilon^2$, where A_{11} is a positive constant that does not depend on θ. On the other hand, C_{22} is positive for $\theta = \theta_c$ since parallel-mode ripples are observed to form above the threshold. Equation (38) may now be written

$$J^{-1}U_T = -A_{11} U_{XX} + C_{22} U_{YY} + C_{1111} U_{XXXX} + \lambda_1 U_X^2. \quad (39)$$

Notice that ϵ does not appear in Eq. (39). Thus, the scaling we posited in Eqs. (9) and (10) leads to a well-behaved EOM in the small-ϵ limit. Moreover, all of the terms are of the same order in ϵ.

The EOM (38) becomes

$$J^{-1}u_t = C_{11} u_{xx} + C_{22} u_{yy} + C_{1111} u_{xxxx} + \lambda_1 u_x^2 \quad (40)$$

when written in terms of the unscaled variables. Equation (40) is the simplified AKS equation that we set out to derive. Note that we must have $C_{1111} < 0$, since otherwise arbitrarily short wavelengths are unstable and the continuum description breaks down.

As is well known, if the initial condition for the AKS equation (40) is low-amplitude spatial white noise and $C_{11} < 0$, the interface width grows exponentially with time at short times. At long times, the ripple amplitude saturates and the solution exhibits spatiotemporal chaos.

Equation (39) can be reduced to a parameter-free form by rescaling. We define the dimensionless variables

$$\tilde{X} = \mathrm{sgn}(C_{111})\left(\frac{A_{11}}{|C_{1111}|}\right)^{1/2} X, \quad \tilde{Y} = \frac{A_{11}}{(C_{22}|C_{1111}|)^{1/2}} Y, \quad \tilde{T} = \frac{JA_{11}^2}{|C_{1111}|} T, \quad \text{and} \quad \tilde{U} = \frac{\lambda_1}{A_{11}} U, \quad (41)$$

where $\mathrm{sgn}(C_{111})$ denotes the sign of C_{111}. We obtain

$$\tilde{U}_{\tilde{T}} = -\tilde{U}_{\tilde{X}\tilde{X}} + \tilde{U}_{\tilde{Y}\tilde{Y}} - \tilde{U}_{\tilde{X}\tilde{X}\tilde{X}\tilde{X}} + \tilde{U}_{\tilde{X}}^2. \quad (42)$$

For Eq. (42) to apply, the target material must be elemental, there must be diametrically opposed beams of obliquely incident noble gas ions, θ must be close to the critical angle θ_c, and the time must be sufficiently long. It is remarkable that Eq. (42) is valid for any elemental target material, noble gas ion species, and ion energy.

A simulation of Eq. (42) with a low-amplitude spatial white noise initial condition is shown in Figs. 1(a)–1(c). (For details of the method of numerical integration employed, see Ref. [22].) Solutions to Eq. (42) with initial conditions of this kind develop disordered parallel-mode ripples with a wavelength of order 1 and the ripple amplitude saturates at a value of order 1. The time needed for the steady-state ripple amplitude to be approached is also of order 1. To describe transverse correlations, we define the long-time transverse correlation function

$$C(\Delta\tilde{Y}) \equiv \lim_{\tilde{T}\to\infty} \iint [\tilde{U}(\tilde{X},\tilde{Y},\tilde{T}) - \langle \tilde{U}(\tilde{T})\rangle][\tilde{U}(\tilde{X},\tilde{Y}+\Delta\tilde{Y},\tilde{T}) - \langle \tilde{U}(\tilde{T})\rangle]\, d\tilde{X}\, d\tilde{Y}, \quad (43)$$

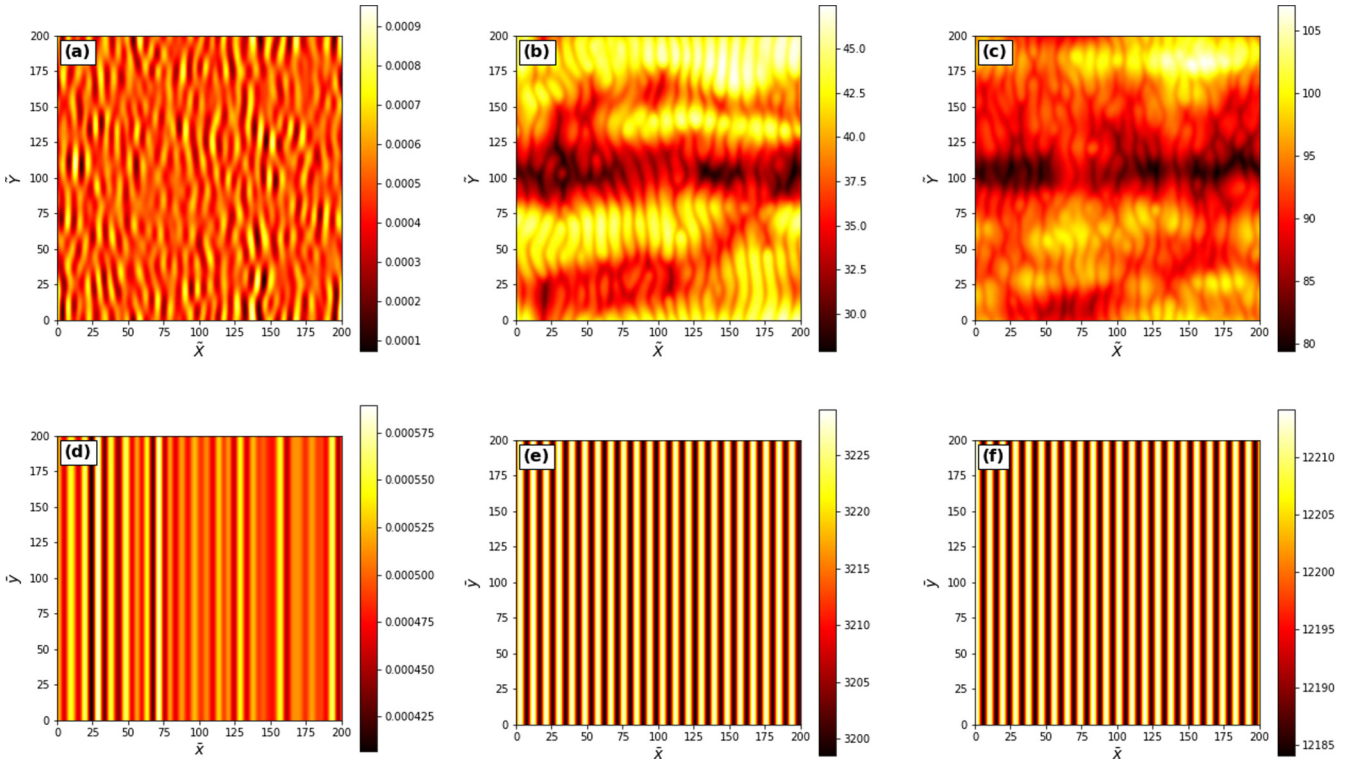

FIG. 1. $\tilde{U}$ vs $\tilde{X}$ and $\tilde{Y}$ for dimensionless times (a) $\tilde{T} = 10$, (b) $\tilde{T} = 100$, and (c) $\tilde{T} = 200$ for the EOM (42). $\bar{u}$ vs $\bar{x}$ and $\bar{y}$ for dimensionless times (d) $\bar{t} = 10$, (e) $\bar{t} = 100$, and (f) $\bar{t} = 200$ for the EOM (49) with $\alpha = 50$. The initial condition was low-amplitude spatial white noise and the domain size was 200×200 in both simulations.

where $\langle \tilde{U}(\tilde{T}) \rangle$ is the spatial average of $\tilde{U}$ at time $\tilde{T}$. $C(\Delta\tilde{Y})$ decays toward zero with a characteristic transverse length scale of order 1. It follows that in the original, unscaled problem, the ripple wavelength diverges as $\epsilon^{-1} = (\theta - \theta_c)^{-1/2}$ as θ approaches θ_c from above. Similarly, as $\theta \to \theta_c^+$, the saturation value of the ripple amplitude, the time for the ripple amplitude to saturate, and the transverse correlation length scale like $\theta - \theta_c$, $(\theta - \theta_c)^{-2}$, and $(\theta - \theta_c)^{-1}$, respectively. Testing these predictions experimentally will be challenging, since as θ approaches the threshold value θ_c from above, the ripple wavelength diverges, the long-time ripple amplitude tends to zero, and the time needed for the ripple amplitude to saturate diverges. Nevertheless, similar challenges were successfully overcome in experimental tests of the scaling behavior predicted by the renormalization group for critical phenomena in equilibrium statistical systems. One encouraging sign is that the experiments reported in Ref. [15] provide evidence for a divergence in the ripple wavelength l as θ is reduced toward θ_c. More refined measurements could show whether l diverges like $(\theta - \theta_c)^{-1/2}$, as predicted.

We obtained the EOM (39) by expanding to order ϵ^6. If we instead expand to order ϵ^8, we recover Eq. (39), but with correction terms of order ϵ^2:

$$J^{-1}U_T = -A_{11}U_{XX} + C_{22}U_{YY} + C_{1111}U_{XXXX} + \lambda_1 U_X^2 + \epsilon^2\big(C_{1122}U_{XXYY} + \lambda_2 U_Y^2 + \mu_1 \partial_X^2 U_X^2 + \mu_2 U_{XX}^2 + \mu_3 U_{XXXXXX}\big). \quad (44)$$

The coefficients C_{1122}, λ_2, μ_1, μ_2, and μ_3 can be related to crater function moments if desired.

Close to threshold, ϵ is small and the correction terms in Eq. (44) can safely be neglected. However, as θ is increased, the correction terms gain in importance. The most commonly used EOM is the AKS equation (1). It is interesting to note that, close to threshold, the terms proportional to U_Y^2 and U_{XXYY} that are ordinarily included in the AKS equation are in fact small corrections. At the same time, terms proportional to $\partial_X^2 U_X^2$, U_{XX}^2, and U_{XXXXXX} are usually not included in the EOM, even though they are of the same order as U_Y^2 and U_{XXYY}. The term proportional to U_{YYYY} that appears in the AKS equation is an even higher order correction that would appear in the EOM (44) with a coefficient of order ϵ^4.

The term $\partial_X^2 U_X^2$ in Eq. (44) is the so-called conserved Kuramoto-Sivashinsky nonlinearity, and its influence on the dynamics has been studied [17–19]. The effect of the term U_{XX}^2 has also been investigated [32]. So far as we are aware, the effect of the term $\epsilon\mu_3 U_{XXXXXX}$ has not yet been studied, but, if $\mu_3 > 0$, it is an additional long-wavelength smoothing term whose effect is expected to be modest.

VI. EQUATION OF MOTION FOR A SINGLE INCIDENT BEAM

Consider the EOM (34) for a single incident beam with ion flux J. Setting $X' \equiv X + \epsilon^{-3} J C_1 T$ and $T' \equiv T$ and dropping the primes, we obtain

$$J^{-1}U_T = -A_{11}U_{XX} + \epsilon^{-1}C_{111}U_{XXX} + C_{22}U_{YY} + C_{1111}U_{XXXX} + \lambda_1 U_X^2, \quad (45)$$

since $C_{11} = -A_{11}\epsilon^2$. As before, we must have $C_{1111} < 0$. In addition, unless there is a highly unlikely coincidence, C_{111} is nonzero for $\theta = \theta_c$, and we assume that this is the case. In terms of the dimensionless variables defined in Eq. (41), Eq. (45) becomes

$$\tilde{U}_{\tilde{T}} = -\tilde{U}_{\tilde{X}\tilde{X}} + \tilde{U}_{\tilde{Y}\tilde{Y}} - \tilde{U}_{\tilde{X}\tilde{X}\tilde{X}\tilde{X}} + \tilde{U}_{\tilde{X}}^2 + \gamma\epsilon^{-1}\tilde{U}_{\tilde{X}\tilde{X}\tilde{X}}, \quad (46)$$

where

$$\gamma \equiv \frac{|C_{111}|}{(A_{11}|C_{1111}|)^{1/2}} \quad (47)$$

is positive, dimensionless, and of $O(\epsilon^0)$. The dimensionless prefactor γ/ϵ of the linearly dispersive term $\tilde{U}_{\tilde{X}\tilde{X}\tilde{X}}$ in Eq. (46) grows large as θ approaches θ_c from above. This shows that the effect of dispersion becomes crucial close to threshold. Nevertheless, such a term does not appear in the EOM that is typically adopted in the case in which there is a single obliquely incident ion beam, the AKS equation (1).

Recall that $X \equiv \epsilon x$ and $Y \equiv \epsilon^2 y$, and so the rescaling of the longitudinal and transverse coordinates defined by Eq. (41) differs markedly close to threshold. If one were looking at the results of a simulation of Eq. (46) close to threshold, therefore, it would be easy to be seriously misled. To remedy this, we define the new dimensionless variables

$$\bar{x} \equiv \tilde{X} = \mathrm{sgn}(C_{111})\left(\frac{A_{11}}{|C_{1111}|}\right)^{1/2}\epsilon x, \quad \bar{y} \equiv \frac{\gamma A_{11}}{(C_{22}|C_{1111}|)^{1/2}}\epsilon y,$$
$$\bar{t} \equiv \tilde{T}, \quad \text{and} \quad \bar{u} \equiv \tilde{U}. \quad (48)$$

Notice in particular that $\bar{x}$ and $\bar{y}$ are proportional to the same power of ϵ. Equation (45) becomes

$$\bar{u}_{\bar{t}} = -\bar{u}_{\bar{x}\bar{x}} - \bar{u}_{\bar{x}\bar{x}\bar{x}\bar{x}} + \alpha^2\bar{u}_{\bar{y}\bar{y}} + \bar{u}_{\bar{x}}^2 + \alpha\bar{u}_{\bar{x}\bar{x}\bar{x}}, \quad (49)$$

where $\alpha \equiv \gamma/\epsilon$ is large close to threshold.

Equation (49) shows that when α is large, transverse variations in $\bar{u}$ are rapidly suppressed and, to an excellent approximation, we may simply set $\bar{u}_{\bar{y}}$ to zero after an initial transient. This is illustrated by Figs. 1(d)–1(f), which show the time evolution of a numerical solution to Eq. (49) with $\alpha = 50$ and a low-amplitude spatial white noise initial condition. With $\bar{u}_{\bar{y}}$ set to zero, Eq. (49) reduces to

$$\bar{u}_{\bar{t}} = -\bar{u}_{\bar{x}\bar{x}} - \bar{u}_{\bar{x}\bar{x}\bar{x}\bar{x}} + \bar{u}_{\bar{x}}^2 + \alpha\bar{u}_{\bar{x}\bar{x}\bar{x}}. \quad (50)$$

We differentiate Eq. (50) with respect to $\bar{x}$ and set $\tilde{x} = -\bar{x}$, $\tilde{t} = \alpha\bar{t}$, and $v = (2/\alpha)\bar{u}_{\bar{x}}$. This yields

$$v_{\tilde{t}} + \alpha^{-1}(v_{\tilde{x}\tilde{x}} + v_{\tilde{x}\tilde{x}\tilde{x}\tilde{x}}) + vv_{\tilde{x}} + v_{\tilde{x}\tilde{x}\tilde{x}} = 0. \quad (51)$$

Equation (51) is known as the Kawahara equation [33] and has previously been studied as a model of step-bunching dynamics on vicinal surfaces [34,35]. It reduces to the Korteweg–de Vries (KdV) equation

$$v_{\tilde{t}} + vv_{\tilde{x}} + v_{\tilde{x}\tilde{x}\tilde{x}} = 0, \quad (52)$$

a paradigmatic equation in the study of solitons, in the strongly dispersive limit $\alpha \to \infty$. When α is large and finite and the initial condition is low-amplitude spatial white noise, the solution to Eq. (51) tends to a highly ordered steady state that consists of a chain of equally spaced solitons of the same amplitude [33]. This means that when the surface is bombarded with a single ion beam and the angle of incidence, θ, is just above the threshold value, highly ordered parallel-mode ripples form. Indeed, the simulation shown in Figs. 1(d)–1(f) confirms that exceptionally well ordered ripples develop close to threshold. Similarly, simulations of the AKS equation (1) with an additional term $C_{111}u_{xxx}$ appended to the right-hand side show that highly ordered ripples develop when C_{111} is large [22].

Equation (50) does not have a well-defined $\epsilon \to 0$ limit. To obtain an EOM that is well behaved in this limit, we must adopt a different scaling than that given by Eqs. (9) and (10). We now seek solutions to Eq. (8) of the form

$$u(x, y, t) = \epsilon U(X, Y, T), \quad (53)$$

where

$$X \equiv \epsilon x, \quad Y \equiv \epsilon^{3/2} y, \quad \text{and} \quad T \equiv \epsilon^3 t. \quad (54)$$

X, Y, and T are "slow" variables once again, but they are defined differently than in Sec. III. As before, the amplitude of the surface disturbance is small, it varies slowly in space and time, and the spatial variation in the y direction is more gradual than in the x direction for θ close to the critical angle θ_c.

We insert Eq. (53) into Eq. (8) and expand to fifth order in ϵ. The derivation of the EOM is lengthy but proceeds in a fashion that is completely analogous to the derivation given in Sec. IV, and so we omit the details and simply give the final result. We find that

$$\frac{1}{J}U_T = C_{111}U_{XXX} + \lambda_1 U_X^2 + C_{22}U_{YY} + \epsilon\big(-A_{11}U_{XX} + C_{1111}U_{XXXX} + \lambda_2 U_Y^2 + C_{122}U_{XYY} + \beta U_X U_{XX}\big). \quad (55)$$

Once again, the coefficients C_{22}, C_{111}, C_{1111}, and λ_1 are related to the crater function moments through the relations (28), (29), (31), and (32) and $A_{11} = -C_{11}/\epsilon^2$, where C_{11} is given by Eq. (26). Finally,

$$\lambda_2 = -\tfrac{1}{2}M_{2,2}^{0,0}\cos\theta, \quad (56)$$

$$C_{122} = \big(-\tfrac{1}{2}M_1^{0,2} - M_2^{1,1} + M_4^{0,1} + M_5^{1,0} - M_8^{0,0}\big)\cos\theta - \tfrac{1}{2}M^{0,2}\sin\theta, \quad (57)$$

and

$$\beta = \big(M_{1,1}^{1,0} - M_{1,3}^{0,0}\big)\cos\theta - \big(2M_1^{1,0} + M_3^{0,0}\big)\sin\theta. \quad (58)$$

Equation (55) is simpler when written in terms of the dimensionless variables

$$\bar{X} \equiv -\mathrm{sgn}(C_{111})\left(\frac{A_{11}}{|C_{1111}|}\right)^{1/2}X, \quad (59)$$

$$\bar{Y} \equiv \frac{|C_{111}|^{1/2}A_{11}^{3/4}}{C_{22}^{1/2}|C_{1111}|^{3/4}}Y, \quad (60)$$

$$\bar{T} \equiv \frac{J|C_{111}|A_{11}^{3/2}}{|C_{1111}|^{3/2}}T, \quad (61)$$

and

$$\bar{U} = -\frac{\lambda_1|C_{1111}|^{1/2}}{|C_{111}|A_{11}^{1/2}}U. \quad (62)$$

We obtain

$$\bar{U}_{\bar{T}} = -\bar{U}_{\bar{X}\bar{X}\bar{X}} - \bar{U}_{\bar{X}}^2 + \bar{U}_{\bar{Y}\bar{Y}} - \gamma^{-1}\epsilon\big(\bar{U}_{\bar{X}\bar{X}} + \bar{U}_{\bar{X}\bar{X}\bar{X}\bar{X}} + \nu_1\bar{U}_{\bar{Y}}^2 + \nu_2\bar{U}_{\bar{X}\bar{Y}\bar{Y}} + \nu_3\bar{U}_{\bar{X}}\bar{U}_{\bar{X}\bar{X}}\big). \quad (63)$$

Here

$$\nu_1 \equiv \frac{\lambda_2 C_{111}^2}{\lambda_1 C_{22}|C_{1111}|}, \quad (64)$$

$$\nu_2 \equiv \frac{C_{111}C_{122}}{C_{22}|C_{1111}|}, \quad (65)$$

and

$$\nu_3 \equiv -\frac{\beta C_{111}}{\lambda_1|C_{1111}|} \quad (66)$$

are dimensionless constants.

Equation (63) shows that linear dispersion is important close to threshold and at long times when a single ion beam is incident on the surface, just as we found earlier in this section. Moreover, several of the terms that are normally included in the EOM are in fact small corrections in this case. In particular, terms proportional to $\bar{U}_{\bar{X}\bar{X}}$, $\bar{U}_{\bar{X}\bar{X}\bar{X}\bar{X}}$, and $\bar{U}_{\bar{Y}}^2$ appear in the AKS equation (1), but Eq. (63) shows that their influence on the dynamics is small. In addition, terms proportional to $\bar{U}_{\bar{X}\bar{Y}\bar{Y}}$ and $\bar{U}_{\bar{X}}\bar{U}_{\bar{X}\bar{X}}$ are of the same order in ϵ as the terms proportional to $\bar{U}_{\bar{X}\bar{X}}$, $\bar{U}_{\bar{X}\bar{X}\bar{X}\bar{X}}$, and $\bar{U}_{\bar{Y}}^2$, but the former terms are not included in the AKS equation. The AKS equation is therefore an inconsistent approximation to the dynamics at long times and for θ just above θ_c if a single beam is incident upon the surface.

We sought solutions to the EOM (8) of the form given by Eqs. (53) and (54) and so reduced the EOM to Eq. (63). If the initial form of the surface $u(x, y, 0)$ is not a slowly varying function of x and y and its amplitude is smaller than $O(\epsilon^1)$, there will be an early time, transient regime in which the dynamics is not well described by Eq. (63). This will be the case if the initial surface is low-amplitude spatial white noise, the initial condition most commonly adopted in simulations. For such an initial condition, the influence of terms proportional to u_{xx}, u_{xxxx}, u_{xxyy}, and u_{yyyy} could be important at short times. Once the short-wavelength Fourier modes have been sufficiently suppressed and the amplitude of the surface disturbance has grown to be of order ϵ, Eq. (63) will provide a good description of the dynamics.

Close to threshold, we may drop the terms of $O(\epsilon)$ from Eq. (63) to obtain

$$\bar{U}_{\bar{T}} + \bar{U}_{\bar{X}}^2 + \bar{U}_{\bar{X}\bar{X}\bar{X}} = \bar{U}_{\bar{Y}\bar{Y}}. \quad (67)$$

This equation has only four terms and no free parameters. Conditions for the validity of the EOM (67) are few: the target material must be elemental, there must be a single beam of obliquely incident noble gas ions, θ must be close to the critical angle θ_c, and the time must be sufficiently long. This EOM therefore has a remarkably high degree of universality.

Taking the derivative of Eq. (67) with respect to $\bar{X}$ and setting $V = 2\bar{U}_{\bar{X}}$, we obtain

$$V_{\bar{T}} + VV_{\bar{X}} + V_{\bar{X}\bar{X}\bar{X}} = V_{\bar{Y}\bar{Y}}. \quad (68)$$

If V does not depend on the transverse coordinate $\bar{Y}$, Eq. (68) reduces to the KdV equation. Equation (68) is therefore a generalization of the KdV equation to the $(2+1)$-dimensional case in which V depends on $\bar{Y}$ as well as $\bar{X}$ and $\bar{T}$. As far as we have been able to determine, it has not previously been studied, although two other $(2+1)$-dimensional generalizations of the KdV equation, the Kadomtsev-Petviashvili [36] and Zakharov-Kuznetsov equations [37], have been studied in great depth [38].

Equation (68) raises the exciting possibility that solitons could be observed on the surface of an ion-bombarded solid surface close to the threshold for pattern formation. Solitons are surface disturbances that propagate without changing their form [39]. Because their velocity of propagation depends on their amplitude, pairs of solitons can collide. After they do so, they very nearly return to their original form. A shift in the positions of the solitons relative to where they would have been had no collision occurred is the only easily discernible evidence that a collision took place.

Equation (68) has the soliton solution given by

$$V(\bar{X}, \bar{Y}, \bar{T}) = 12A^2\mathrm{sech}^2(A(\bar{X} - \bar{X}_0 - 4A^2\bar{T})), \quad (69)$$

where A is a positive constant and the arbitrary real constant $\bar{X}_0$ gives the location of the soliton at time $\bar{T} = 0$. Since $V = 2\bar{U}_{\bar{X}}$, the scaled surface height $\bar{U}$ is given by

$$\bar{U}(\bar{X}, \bar{Y}, \bar{T}) = 6A\tanh(A(\bar{X} - \bar{X}_0 - 4A^2\bar{T})) + \bar{U}_0, \quad (70)$$

where $\bar{U}_0$ is a constant of integration that we may set to zero. Equation (70) shows that the soliton solution is a smoothed step on the solid surface with height $\Delta\bar{U} \equiv 12A$. The step propagates with constant velocity without changing its form and is oriented perpendicularly to the incident ion beam. Its width is inversely proportional to the step height $\Delta\bar{U}$. The soliton's propagation velocity, on the other hand, is proportional to $(\Delta\bar{U})^2$.

VII. DISCUSSION

In derivations of the equation of motion for an ion-sputtered surface that took the Sigmund model as their starting point, it was assumed that the amplitude of the surface disturbance is small and that the surface height varies slowly with position [11,13,14]. Expansions were then carried out in which terms of various orders in u and the spatial derivatives ∂_x and ∂_y were retained. In the case of the AKS equation (1), for example, terms that are linear in u and up to fourth order in the spatial derivatives, as well as terms that are second order in both u and the space derivatives, are included in the EOM [13,14]. It is unclear whether the discarded terms are actually negligible, however. There is experimental evidence that "higher-order" terms like $\partial_x^2 u_x^2$ and u_x^3 can in certain circumstances play important roles [17–21]. The conserved Kuramoto-Sivashinsky (CKS) nonlinearity $\partial_x^2 u_x^2$, for example, is likely responsible for the ripple coarsening that is often observed in experiments [17–19].

In this paper, we studied the behavior of an ion-sputtered solid surface for angles of incidence, θ, just above the threshold angle for ripple formation, θ_c. We carried out a systematic expansion in powers of the small parameter $\epsilon \equiv (\theta - \theta_c)^{1/2}$ and retained all terms up to a given order in ϵ. In the case of two diametrically opposed incident beams, the EOM close to

threshold and at sufficiently long times is the simplified AKS equation (40).

The case in which diametrically opposed beams are simultaneously incident on the solid surface is relatively simple because the EOM must be invariant under the transformation $x \to -x$. In an experiment, two ion beams would not actually be used. Instead, the sample would be rotated periodically through 180° increments about the z axis while being bombarded with a single obliquely incident beam. If the time between rotations were made sufficiently small, the effect would be essentially the same as if the sample were concurrently bombarded with diametrically opposed beams.

When the surface is bombarded with a single obliquely incident beam, the linearly dispersive term u_{xxx} plays a crucial role close to threshold and fundamentally alters the behavior. Highly ordered ripples can emerge at sufficiently long times. This is an exciting finding because there is a high density of defects in the patterns that are typically formed by ion sputtering, and this issue has arguably been the primary obstacle that has prevented the widespread use of ion bombardment as a nanofabrication tool.

In deriving the EOM for an ion-sputtered solid surface, we used a generalized crater function formalism. To this point, the CFF has primarily been regarded as a tool that takes input from atomistic simulations to produce estimates of the coefficients in a given equation of motion. In this paper, we adopted a different perspective: we used a generalized CFF to derive the equation of motion. A by-product of this derivation is expressions that relate the coefficients in the EOM to moments of the crater function. These expressions could be used to obtain estimates of the coefficients in the EOM from input produced by atomistic simulations.

As was noted in the pioneering work of Norris *et al.*, the crater function depends on the shape of the entire surface [25]. In their 2011 paper, however, Norris and co-workers neglected the dependence of the crater on the form of the surface [15]. Harrison and Bradley later took into account the effect that the surface curvature at the point of impact has on the crater [26], which led to corrected expressions for the coefficients C_{11} and C_{22}. In the present work, the dependence of the crater function on spatial derivatives of u of arbitrarily high order was included. This is equivalent to taking into account the dependence of the crater on the form of the whole surface. We demonstrated that, to lowest nontrivial order in ϵ, only the dependence of the crater on spatial derivatives of u up to the fourth order affects the equation of motion [see Eqs. (24), (26), (28), (29), (31), and (32)].

In previous treatments of the CFF, approximations to the form of the surface were employed in determining the effect of impinging ions on the surface velocity h_t at the origin [16,25,26]. These approximations, which are accurate only in the immediate vicinity of the origin, were argued to be reasonable because only ions impacting the surface within a distance on the order of the ion range a contribute significantly to h_t, and the surface height varies little over distances on the order of a. Norris and co-workers [25] and Harrison and Bradley [26] performed a Taylor-series expansion of the surface height h about the origin and retained terms up to second order in x and y. Some terms of higher order were subsequently included by Hofsäss and Bobes [16], but, as we show in the Appendix, the expressions that they found for the coefficients C_{111} and C_{1111} are incorrect. In the present paper, terms of all orders were retained in the Taylor-series expansion.

In the CFFs of Norris and co-workers [25] and of Harrison and Bradley [26], the equation of motion was linearized; i.e., only terms of first order in u were retained. Hofsäss and Bobes included terms up to third order in u in the EOM [16]. Terms of all orders in u were retained in the present work. However, close to the threshold for pattern formation, only terms of second order in u appear in the EOM to lowest nontrivial order in ϵ.

As the preceding discussion shows, in all previous versions of the CFF, two different expansions were carried out and the resulting series were truncated at some order. It was not apparent whether the discarded terms were indeed smaller than those that were retained in the EOM, or whether terms that are negligibly small were included in the EOM when they ought to have been dropped. In contrast, in this paper, we carried out a systematic expansion in the small parameter ϵ and retained all terms in the EOM up to a given order in ϵ. In this way, we made the CFF internally consistent and placed it on a solid mathematical foundation.

Our crater function f is to be evaluated at a time long enough after the ion impact that essentially all ion-induced motion has ceased. It therefore takes into account all of the effects of the ion impact, including sputtering, ballistic mass redistribution, and ion-induced surface viscous flow. In contrast, in the CFF introduced by Norris *et al.* [25], the crater includes only the short-time or "prompt" effects of the ion impact that occur within picoseconds after the arrival of the impinging ion. The effects of ion-induced viscous flow were assumed to occur over much longer time scales and were handled separately.

Craters computed in atomistic simulations that include only the prompt effects of the ion impacts could be used to compute the contributions of sputtering and ion-induced mass redistribution to the coefficients in the EOMs (35), (40), and (55) using Eqs. (24), (26), (28), (29), (31), (32), and (56)–(58). The contributions of ion-induced viscous flow or thermally activated surface diffusion to these coefficients would then have to be inferred from experiment or be computed by other means, as in past work [15]. These contributions are expected to be significant only in the case of the coefficient C_{1111}.

We assumed that when a broad beam is incident on the surface, the ion flux is low enough that essentially all ion-induced motion near a point of ion impact, **P**, has ceased before another ion strikes the surface in the immediate vicinity of **P**. The hydrodynamic theory developed by Cuerno and co-workers, on the other hand, applies in the high-flux regime in which a layer at the surface of the target is mobilized by the ion impacts [40–42]. In that theory, it is assumed that the entire layer is continuously in motion and that it behaves like a highly viscous fluid. In another theory that would also apply only for sufficiently high ion fluxes, a layer at the surface of the target is modeled as a viscous or viscoelastic medium into which the ion beam continually injects biaxial compressive stress [43,44].

Although we found that terms proportional to $\partial_x^2 u_x^2$ and u_x^3 have a negligible effect on the dynamics close to the threshold

for pattern formation, the effect of these and other terms could be substantial away from threshold. As we have already noted, the CKS nonlinearity $\partial_x^2 u_x^2$ leads to ripple coarsening, while the cubic nonlinearity u_x^3 can produce terraced surfaces. Both of these phenomena have been observed in experiments. The experiments in which these phenomena were observed were presumably done with angles of incidence, θ, that were well above the critical value θ_c.

VIII. CONCLUSIONS

In this paper, we studied the behavior of an ion-sputtered solid surface for angles of incidence, θ, just above the threshold angle for ripple formation, θ_c. We carried out a systematic expansion in powers of the small parameter $\epsilon \equiv (\theta - \theta_c)^{1/2}$ and retained all terms up to a given order in ϵ. In the case of two diametrically opposed incident beams, the equation of motion close to threshold and at sufficiently long times is a simplified AKS equation. We also determined the long-time, near-threshold scaling behavior of the rippled surface's wavelength, transverse correlation length, and amplitude.

When the surface is bombarded with a single obliquely incident beam, linear dispersion plays a crucial role close to threshold and fundamentally alters the behavior. Highly ordered ripples can emerge at sufficiently long times. This is an exciting finding because there is a high density of defects in the patterns that are typically formed by ion sputtering, and this issue has arguably been the primary obstacle that has prevented the widespread use of ion bombardment as a nanofabrication tool. We also find that solitons can propagate over the solid surface.

In our derivations of the EOMs for the single and dual beam cases, we utilized a generalized crater function formalism. Our crater function formalism yields explicit expressions for the coefficients that appear in the equations of motion that apply in the single beam and dual beam cases. These expressions relate the coefficients to moments of the crater function. Importantly, our treatment places the CFF on a firm mathematical footing and generalizes earlier formulations.

ACKNOWLEDGMENTS

I thank Kevin M. Loew for the simulation results and Patrick D. Shipman, Mark Hoefer, Hans Hofsäss, and Mark Ablowitz for valuable discussions. This work was supported by Grant No. DMS-1814941 from the U.S. National Science Foundation.

APPENDIX

Our crater function formalism yielded expressions for the coefficients C_1, C_{11}, C_{22}, C_{111}, C_{1111}, and λ_1 in the EOMs (35) and (55) in terms of the moments of the crater function $f = f(x, y, \theta; h_x, h_y, h_{xx}, h_{xy}, h_{yy}, \ldots)$: see Eqs. (24), (26), (28), (29), (31), and (32). However, when atomistic simulations are used to estimate crater function moments, it is the moments of the crater function $F = F(x, y, \theta; h_{xx}, h_{xy}, h_{yy}, h_{xxx}, \ldots)$ that are computed [15,16]. This is more computationally efficient because it is then only necessary to simulate ion impacts on surfaces with slope zero at the point of impact. We will therefore rewrite our expressions for the coefficients entirely in terms of moments of F in this Appendix. In addition to making our results more useful for the task of estimating coefficients using input from atomistic simulations, this will allow us to show that our expressions for C_1, C_{11}, C_{22}, and λ_1 agree with results obtained elsewhere [20,26].

We begin by defining the moments of the crater function F that we need. Let

$$F_0(x, y, \theta) \equiv F(x, y, \theta; 0, 0, \ldots), \tag{A1}$$

$$F_1(x, y, \theta) \equiv \frac{\partial}{\partial h_{xx}} F(x, y, \theta; h_{xx}, 0, 0, \ldots)\Big|_{h_{xx}=0}, \tag{A2}$$

$$F_2(x, y, \theta) \equiv \frac{\partial}{\partial h_{xy}} F(x, y, \theta; 0, h_{xy}, 0, 0, \ldots)\Big|_{h_{xy}=0}, \tag{A3}$$

and so forth. Similarly, for positive integers i and j, $F_{i,j}(x, y, \theta)$ denotes the partial derivative of $F = F(x, y, \theta; h_{xx}, h_{xy}, h_{yy}, \ldots)$ with respect to the ith and jth arguments that appear after the semicolon, evaluated for all the arguments after the semicolon set equal to zero. We define the crater function moments

$$\mathcal{M}^{n,m} \equiv \iint x^n y^m F_0(x, y, \theta)\, dx\, dy, \tag{A4}$$

$$\mathcal{M}_i^{n,m} \equiv \iint x^n y^m F_i(x, y, \theta)\, dx\, dy, \tag{A5}$$

and

$$\mathcal{M}_{i,j}^{n,m} \equiv \iint x^n y^m F_{i,j}(x, y, \theta)\, dx\, dy \tag{A6}$$

for nonnegative integers n and m and positive integers i and j. These are the moments that were employed in prior formulations of the CFF.

Equation (7) shows that $f_0(x, y, \theta) = F_0(x, y, \theta)$ and hence

$$M^{n,m} = \mathcal{M}^{n,m} \tag{A7}$$

for nonnegative integers n and m. Similarly, $M_i^{n,m}$ can readily be written in terms of moments of F provided that $i > 2$. For example,

$$\begin{aligned} M_3^{n,m} &= \iint x^n y^m \frac{\partial}{\partial h_{xx}} f(x, y, \theta; 0, 0, h_{xx}, 0, 0, \ldots)\Big|_{h_{xx}=0} dx\, dy \\ &= \iint x^n y^m \frac{\partial}{\partial h_{xx}} F(x, y, \theta; h_{xx}, 0, 0, \ldots)\Big|_{h_{xx}=0} dx\, dy \\ &= \mathcal{M}_1^{n,m}. \end{aligned} \tag{A8}$$

The general result is

$$M_i^{n,m} = \mathcal{M}_{i-2}^{n,m} \tag{A9}$$

for $i > 2$.

We now show that

$$M_1^{n,0} = -\frac{\partial}{\partial \theta} \mathcal{M}^{n,0} \tag{A10}$$

for all n and that

$$M_2^{0,1} = -\mathcal{M}^{1,0} \cot\theta. \tag{A11}$$

To that end, consider an ion impact at the origin on the surface given by $h(x, y) = S_1 x + S_2 y$, where S_1 and S_2 are

small constants. On average, the surface after the ion impact is

$$h(x,y) = S_1 x + S_2 y - f(x,y,\theta;S_1,S_2,0,0,\ldots) \tag{A12}$$

relative to the coordinate system (x,y,z). Relative to the coordinate system (ξ,η,ζ), it is given by

$$H(\xi,\eta) = -F(\xi,\eta,\phi;0,0,\ldots), \tag{A13}$$

where the local angle of incidence, ϕ, is given by $\cos\phi = \hat{\boldsymbol{e}}\cdot\hat{\boldsymbol{n}}$. We work to first order in S_1 and S_2 in what follows. To that order [26],

$$\hat{\boldsymbol{t}}_\xi = \hat{\boldsymbol{x}} - (S_2\cot\theta)\hat{\boldsymbol{y}} + S_1\hat{\boldsymbol{z}}, \tag{A14}$$

$$\hat{\boldsymbol{t}}_\eta = (S_2\cot\theta)\hat{\boldsymbol{x}} + \hat{\boldsymbol{y}} + S_2\hat{\boldsymbol{z}}, \tag{A15}$$

and

$$\hat{\boldsymbol{n}} = -S_1\hat{\boldsymbol{x}} - S_2\hat{\boldsymbol{y}} + \hat{\boldsymbol{z}}. \tag{A16}$$

For any point on the surface $\boldsymbol{r}$, we have

$$\boldsymbol{r} = x\hat{\boldsymbol{x}} + y\hat{\boldsymbol{y}} + h(x,y)\hat{\boldsymbol{z}} = \xi\hat{\boldsymbol{t}}_\xi + \eta\hat{\boldsymbol{t}}_\eta + H(\xi,\eta)\hat{\boldsymbol{n}}. \tag{A17}$$

Therefore,

$$\xi = \boldsymbol{r}\cdot\hat{\boldsymbol{t}}_\xi = x - (S_2\cot\theta)y, \tag{A18}$$

$$\eta = \boldsymbol{r}\cdot\hat{\boldsymbol{t}}_\eta = (S_2\cot\theta)x + y, \tag{A19}$$

and

$$H(\xi,\eta) = \boldsymbol{r}\cdot\hat{\boldsymbol{n}} = -S_1 x - S_2 y + h(x,y). \tag{A20}$$

We now insert Eqs. (A12) and (A13) into Eq. (A20). This yields

$$F(\xi,\eta,\phi;0,0,\ldots) = f(x,y,\theta;S_1,S_2,0,0,\ldots). \tag{A21}$$

Using Eq. (A16), we find that $\cos\phi = \hat{\boldsymbol{e}}\cdot\hat{\boldsymbol{n}} = \cos\theta + S_1\sin\theta$ to first order and hence $\phi = \theta - S_1$ to that order. Equation (A21) becomes

$$F(\xi,\eta,\theta - S_1;0,0,\ldots) = f(x,y,\theta;S_1,S_2,0,0,\ldots). \tag{A22}$$

We are now prepared to show that Eq. (A10) is valid. We begin by setting S_2 to zero. Using Eqs. (A18), (A19), and (A22), we obtain

$$\begin{aligned}\frac{\partial}{\partial\theta}\mathcal{M}^{n,0} &= \frac{\partial}{\partial\theta}\iint F(x,y,\theta;0,0,\ldots)x^n\,dx\,dy\\ &= -\iint\frac{\partial}{\partial S_1}F(x,y,\theta - S_1;0,0,\ldots)\Big|_{S_1=0}x^n\,dx\,dy\\ &= -\iint\frac{\partial}{\partial S_1}f(x,y,\theta;S_1,0,0,\ldots)\Big|_{S_1=0}x^n\,dx\,dy\\ &= -M_1^{n,0},\end{aligned} \tag{A23}$$

as required. Another relation we need,

$$M_{1,1}^{0,0} = \frac{\partial^2}{\partial\theta^2}\mathcal{M}^{0,0}, \tag{A24}$$

is derived in much the same fashion.

To establish the validity of Eq. (A11), we set $S_1 = 0$ and consider small, nonzero S_2. By definition,

$$M_2^{0,1} = \frac{\partial}{\partial S_2}\int dx\int dy f(x,y,\theta;0,S_2,0,0,\ldots)y\Big|_{S_2=0}.$$

We obtain $y = \eta - (S_2\cot\theta)\xi$ from Eqs. (A18) and (A19). Utilizing Eq. (7) and Eq. (A22) with $S_1 = 0$, we find that

$$\begin{aligned}M_2^{0,1} &= \frac{\partial}{\partial S_2}\int d\xi\int d\eta F(\xi,\eta,\theta;0,0,\ldots)\\ &\quad\times[\eta - (S_2\cot\theta)\xi]\Big|_{S_2=0}\\ &= -\cot\theta\int d\xi\int d\eta F(\xi,\eta,\theta;0,0,\ldots)\xi\\ &= -\mathcal{M}^{1,0}\cot\theta,\end{aligned}$$

which is the required relation.

Using Eqs. (A7), (A9)–(A11), and (A24), Eqs. (24), (26), (28), (29), (31), and (32) become

$$C_1 = \frac{\partial}{\partial\theta}(\mathcal{M}^{0,0}\cos\theta), \tag{A25}$$

$$C_{11} = -\frac{\partial}{\partial\theta}(\mathcal{M}^{1,0}\cos\theta) - \mathcal{M}_1^{0,0}\cos\theta, \tag{A26}$$

$$C_{22} = -\mathcal{M}^{1,0}\cot\theta\cos\theta - \mathcal{M}_3^{0,0}\cos\theta, \tag{A27}$$

$$C_{111} = \frac{1}{2}\frac{\partial}{\partial\theta}(\mathcal{M}^{2,0}\cos\theta) + \left(\mathcal{M}_1^{1,0} - \mathcal{M}_4^{0,0}\right)\cos\theta, \tag{A28}$$

$$\begin{aligned}C_{1111} &= -\frac{1}{6}\frac{\partial}{\partial\theta}(\mathcal{M}^{3,0}\cos\theta)\\ &\quad + \left(-\frac{1}{2}\mathcal{M}_1^{2,0} + \mathcal{M}_4^{1,0} - \mathcal{M}_8^{0,0}\right)\cos\theta,\end{aligned} \tag{A29}$$

and

$$\lambda_1 = \sin\theta\frac{\partial}{\partial\theta}\mathcal{M}^{0,0} - \frac{1}{2}\cos\theta\frac{\partial^2}{\partial\theta^2}\mathcal{M}^{0,0}. \tag{A30}$$

Equations (A25)–(A30) give the coefficients in the EOM (35) exclusively in terms of the moments of the crater function F, and so we have accomplished the main goal of this Appendix. Equations (A25)–(A27) agree with the results obtained by Harrison and Bradley [26], and our expression for λ_1 [Eq. (A30)] is in accord with the result given by Pearson and Bradley [20]. These results were successfully reproduced by Hofsäss and Bobes [16]. However, our results for C_{111} and C_{1111} do not in general agree with those given in Ref. [16]. The expressions given for these coefficients in Ref. [16] omit the second terms on the right-hand sides of Eqs. (A28) and (A29). This strongly suggests that the dependence of the crater function $F = F(x,y,\theta;h_{xx},h_{xy},h_{yy},h_{xxx},h_{xxy},h_{xyy},h_{yyy},h_{xxxx},\ldots)$ on h_{xx}, h_{xxx}, and h_{xxxx} was overlooked in the derivation of the equations for C_{111} and C_{1111} given in Ref. [16].

[1] For a review, see J. Muñoz-García, L. Vázquez, M. Castro, R. Gago, A. Redondo-Cubero, A. Moreno-Barrado, and R. Cuerno, Mater. Sci. Eng. R **86**, 1 (2014).

[2] S. Facsko, T. Dekorsy, C. Koerdt, C. Trappe, H. Kurz, A. Vogt, and H. L. Hartnagel, Science **285**, 1551 (1999).

[3] F. Frost, A. Schindler, and F. Bigl, Phys. Rev. Lett. **85**, 4116 (2000).

[4] Q. Wei, X. Zhou, B. Joshi, Y. Chen, K.-D. Li, Q. Wei, K. Sun, and L. Wang, Adv. Mater. **21**, 2865 (2009).

[5] M. Fritzsche, A. Muecklich, and S. Facsko, Appl. Phys. Lett. **100**, 223108 (2012).

[6] L. Bischoff, W. Pilz, and B. Schmidt, Appl. Phys. A **104**, 1153 (2011).

[7] L. Bischoff, K.-H. Heinig, B. Schmidt, S. Facsko, and W. Pilz, Nucl. Instrum. Methods Phys. Res. Sect. B **272**, 198 (2012).

[8] R. M. Bradley and P. D. Shipman, Phys. Rev. Lett. **105**, 145501 (2010).

[9] P. D. Shipman and R. M. Bradley, Phys. Rev. B **84**, 085420 (2011).

[10] R. M. Bradley and P. D. Shipman, Appl. Surf. Sci. **258**, 4161 (2012).

[11] R. M. Bradley and J. M. E. Harper, J. Vac. Sci. Technol. A **6**, 2390 (1988).

[12] P. Sigmund, J. Mater. Sci. **8**, 1545 (1973).

[13] R. Cuerno and A.-L. Barabási, Phys. Rev. Lett. **74**, 4746 (1995).

[14] M. A. Makeev, R. Cuerno, and A.-L. Barabási, Nucl. Instrum. Methods Phys. Res. Sect. B **197**, 185 (2002).

[15] S. A. Norris, J. Samela, L. Bukonte, M. Backman, F. Djurabekova, K. Nordlund, C. S. Madi, M. P. Brenner, and M. J. Aziz, Nat. Commun. **2**, 276 (2011).

[16] H. Hofsäss and O. Bobes, Appl. Phys. Rev. **6**, 021307 (2019).

[17] M. Castro, R. Cuerno, L. Vazquez, and R. Gago, Phys. Rev. Lett. **94**, 016102 (2005).

[18] J. Muñoz-García, M. Castro, and R. Cuerno, Phys. Rev. Lett. **96**, 086101 (2006).

[19] J. Muñoz-García, R. Cuerno, and M. Castro, Phys. Rev. B **78**, 205408 (2008).

[20] D. A. Pearson and R. M. Bradley, J. Phys.: Condens Matter **27**, 015010 (2015).

[21] M. P. Harrison, D. A. Pearson, and R. M. Bradley, Phys. Rev. E **96**, 032804 (2017).

[22] K. M. Loew and R. M. Bradley, Phys. Rev. E **100**, 012801 (2019).

[23] M. Cross and H. Greenside, *Pattern Formation and Dynamics in Nonequilibrium Systems* (Cambridge University Press, Cambridge, U.K., 2009).

[24] R. Hoyle, *Pattern Formation: An Introduction to Methods* (Cambridge University Press, Cambridge, U.K., 2007).

[25] S. A. Norris, M. P. Brenner, and M. J. Aziz, J. Phys. Condens. Matter **21**, 224017 (2009).

[26] M. P. Harrison and R. M. Bradley, Phys. Rev. B **89**, 245401 (2014).

[27] G. Carter and V. Vishnyakov, Phys. Rev. B **54**, 17647 (1996).

[28] M. Moseler, P. Gumbsch, C. Casiraghi, A. C. Ferrari, and J. Robertson, Science **309**, 1545 (2005).

[29] B. Davidovitch, M. J. Aziz, and M. P. Brenner, Phys. Rev. B **76**, 205420 (2007).

[30] C. C. Umbach, R. L. Headrick, and K.-C. Chang, Phys. Rev. Lett. **87**, 246104 (2001).

[31] The effect implantation has on the surface dynamics is studied in R. M. Bradley and H. Hofsäss, J. Appl. Phys. **120**, 074302 (2016); H. Hofsäss, K. Zhang, and O. Bobes, *ibid.* **120**, 135308 (2016).

[32] A. J. Bernoff and A. L. Bertozzi, Physica D **85**, 375 (1995).

[33] T. Kawahara, Phys. Rev. Lett. **51**, 381 (1983).

[34] M. Sato and M. Uwaha, Europhys. Lett. **32**, 639 (1995).

[35] C. Misbah and O. Pierre-Louis, Phys. Rev. E **53**, R4318 (1996).

[36] M. J. Ablowitz and P. A. Clarkson, *Solitons: Nonlinear Evolution Equations and Inverse Scattering* (Cambridge University Press, Cambridge, U.K., 1991).

[37] V. E. Zakharov and E. A. Kuznetsov, Sov. Phys. JETP **39**, 285 (1974).

[38] Yet another $(2+1)$-dimensional generalization of the KdV equation is derived and studied in R. M. Bradley, Physica D **158**, 216 (2001).

[39] P. G. Drazin and R. S. Johnson, *Solitons: An Introduction* (Cambridge University Press, Cambridge, U.K., 1989).

[40] M. Castro and R. Cuerno, Appl. Surf. Sci. **258**, 4171 (2012).

[41] M. Castro, R. Gago, L. Vázquez, J. Muñoz-García, and R. Cuerno, Phys. Rev. B **86**, 214107 (2012).

[42] J. Muñoz-García, R. Cuerno, and M. Castro, Phys. Rev. B **100**, 205421 (2019).

[43] S. A. Norris, Phys. Rev. B **85**, 155325 (2012).

[44] S. A. Norris, Phys. Rev. B **86**, 235405 (2012).